PROCEEDINGS OF SCIENCE

Nucleon electromagnetic and axial form factors with N_f=2 twisted mass fermions at the physical point

Constantia Alexandrou
Department of Physics, University of Cyprus, P.O. Box 20537, 1678 Nicosia, Cyprus and Computation-based Science and Technology Research Center, The Cyprus Institute, 20 Konstantinou Kavafi Str., 2121 Nicosia, Cyprus
E-mail: alexand@ucy.ac.cy

Martha Constantinou
Department of Physics, Temple University, Philadelphia, PA
E-mail: marthac@temple.edu

Kyriakos Hadjiyiannakou, Christos Kallidonis, Giannis Koutsou*
Computation-based Science and Technology Research Center, The Cyprus Institute, 20 Konstantinou Kavafi Str., 2121 Nicosia, Cyprus
E-mail: k.hadjiyiannakou@cyi.ac.cy, c.kallidonis@cyi.ac.cy, g.koutsou@cyi.ac.cy

Karl Jansen
NIC, DESY, Platanenallee 6, D-15738 Zeuthen, Germany
E-mail: karl.jansen@desy.de

Konstantin Ottnad
Institut für Kernphysik, Johannes Gutenberg-Universität Mainz, Mainz, Germany
*E-mail:*kottnad@uni-mainz.de

Alejandro Vaquero
INFN Sezione di Milano-Bicocca, Milano, Italy
*E-mail:*alexvaq@physics.utah.edu

We present results for the nucleon electromagnetic and axial form factors using an N_f=2 twisted mass fermion ensemble with pion mass of about 131 MeV. We use multiple sink-source separations to identify excited state contamination. Dipole masses for the momentum dependence of the form factors are extracted and compared to experiment, as is the nucleon magnetic moment and charge and magnetic radii.

34th annual International Symposium on Lattice Field Theory
24-30 July 2016
University of Southampton, UK

*Speaker.

PoS(LATTICE2016)154

1. Introduction

Form factors of the nucleon are fundamental probes of its structure. The electromagnetic form factors are related to the nucleon magnetic moment, its electric and magnetic radii. Axial form factors probe chiral symmetry and test partial conservation of the axial current (PCAC), having been studied in chiral effective theories.

Both electromagnetic and axial form factors have been extensively studied in lattice QCD. Recent experimental results, in combination with availability of simulations with physical quark masses on the lattice, have increased interest in an *ab initio* calculation of these form factors. These include tension between the value obtained for the proton radius between electron scattering [1] and hydrogen spectroscopy [2] as well as with recent measurements of muonic deuterium spectroscopy [3]. Furthermore recent re-analyses of neutrino scattering data [4, 5] report large systematics in the determination of the axial dipole mass M_A. In this contribution, we calculate the axial and electromagnetic form factors of the nucleon on an ensemble of twisted mass fermion configurations with clover improvement and two degenerate light quarks ($\mathrm{N_f}=2$) tuned to reproduce a pion mass of about 131 MeV [6]. We use multiple sink-source separations and $\mathscr{O}(10^5)$ statistics to evaluate excited state effects in these quantities.

2. Setup and lattice parameters

2.1 Axial and Electromagnetic form factors

Form factors are extracted from nucleon matrix elements:

$$\langle N(p',s')|\mathscr{O}^X_\mu|N(p,s)\rangle = \sqrt{\frac{m_N^2}{E_N(\vec{p}')E_N(\vec{p})}}\bar{u}_N(p',s')\Lambda^X_\mu(q^2)u_N(p,s)$$

with $N(p,s)$ a nucleon state of momentum p and spin s, $E_N(\vec{p})=p_0$ its energy and m_N its mass, $q=p'-p$, the momentum transfer from initial (p) to final (p') momentum, u_N a nucleon spinor and $\mathscr{O}^X$ either the axial ($X=A$) or vector ($X=V$) current. For the case of axial form factors, we use the axial current: $\mathscr{O}^A_\mu = A^3_\mu = \bar{\psi}\frac{\tau_3}{2}\gamma_5\gamma_\mu\psi$, with $\bar{\psi}=(\bar{u},\bar{d})$, u and d up- and down-quark fields and τ_3 the third Pauli matrix acting on flavor space. For the electromagnetic form factors we use the isovector, symmetrized lattice conserved vector current $\mathscr{O}^V_\mu = \frac{1}{2}[j_\mu(x)+j_\mu(x-\hat{\mu})]$, with $j_\mu(x)$ the Wilson conserved current. Use of the isovector current means that disconnected contributions cancel. Furthermore, use of the conserved electromagnetic current means no renormalization of the vector operator is required. For the axial form factors we use Z_A =0.7910(4)(5) [7]. The matrix element of the axial current yields the axial G_A and induced pseudo-scalar G_p form factors, while the vector current yields the Dirac F_1 and Pauli F_2 form factors:

$$\Lambda^A_\mu(q^2) = \frac{i}{2}\gamma_5\gamma_\mu G_A(q^2) + \frac{q_\mu\gamma_5}{2m_N}G_p(q^2), \quad \Lambda^V_\mu(q^2) = \gamma_\mu F_1(q^2) + \frac{i\sigma_{\mu\nu}q^\nu}{2m_N}F_2(q^2). \tag{2.1}$$

The Dirac and Pauli form factors can also be expressed in terms of the nucleon electric G_E and magnetic G_M Sachs form factors via $G_E(q^2) = F_1(q^2) + \frac{q^2}{(2m_N)^2}F_2(q^2)$ and $G_M(q^2) = F_1(q^2) + F_2(q^2)$.

PoS(LATTICE2016)154

2.2 Lattice extraction of form factors

On the lattice, extraction of matrix elements requires calculating a three-point correlation function. We use sequential inversions through the sink fixing the sink momentum $\vec{p}'$ to zero, which constrains $\vec{p} = -\vec{q}$. We form a ratio of three- to two-point functions which, after taking the large time limit, cancel unknown overlaps and energy exponentials: $R_\mu(\Gamma;\vec{q};t_s;t_{\rm ins}) \xrightarrow[t_{\rm ins}\gg]{t_s - t_{\rm ins}\gg} \Pi_\mu(\Gamma;\vec{q})$, where R_μ is the ratio of three- to two-point functions as defined in Ref. [8], t_s ($t_{\rm ins}$) the sink (insertion) time assuming the source is at the origin, and Γ the sink polarization.

In what follows we will use two methods to extract Π_μ from lattice data: i) in the standard *plateau* method, we fit the $t_{\rm ins}$ dependence of Π_μ to a constant for multiple t_s values observing the dependence with t_s, as shown for G_E in the left panel of Fig. 1. Excited states are suppressed when our result does not change with t_s. ii) in the *summation* method, we calculate: $\sum_{t_{\rm ins}} R_\mu(\Gamma;\vec{q};t_s;t_{\rm ins}) \xrightarrow{t_s\gg} \Pi_\mu(\Gamma;\vec{q})t_s + C$ and carry out a two-parameter fit for obtaining the slope, as in the right panel of Fig. 1.

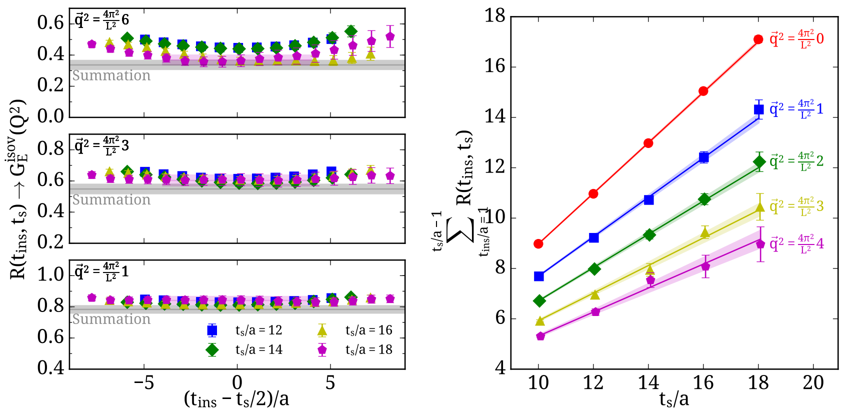

Figure 1: Example fits for G_E, left for the plateau method for three lattice momenta, and right for the summation method for the first five lattice momenta. On the left, with the grey bands, we also show the result of the summation method.

Having $\Pi_\mu(\Gamma;\vec{q})$, different combinations of current insertion directions (μ) and nucleon polarizations determined by Γ yield different form factors. Using Π^V to denote electromagnetic and Π^A for axial matrix elements, we have:

$$\Pi_0^V(\Gamma_0;\vec{q}) = \mathscr{C}\frac{E_N + m_N}{2m_N} G_E(Q^2), \qquad \Pi_i^V(\Gamma_0;\vec{q}) = \mathscr{C}\frac{q_i}{2m_N} G_E(Q^2) \tag{2.2}$$
$$\Pi_i^V(\Gamma_k;\vec{q}) = \mathscr{C}\frac{\varepsilon_{ijk} q_j}{2m_N} G_M(Q^2), \qquad \Pi_i^A(\Gamma_k;\vec{q}) = \frac{i\mathscr{C}}{4m_N}\left[\frac{q_k q_i}{2m_N} G_p(Q^2) - (E_N + m_N)\delta_{ik} G_A(Q^2)\right]$$

where $Q^2 = -q^2$, $\mathscr{C} = \sqrt{\frac{2m_N^2}{E_N(E_N+m_N)}}$, the unpolarized projector: $\Gamma_0 = \frac{1+\gamma_0}{4}$, the polarized projector: $\Gamma_k = i\gamma_5\gamma_k\Gamma_0$, and $i,k = 1,2,3$.

2.3 Lattice setup

We use a lattice with volume $48^3{\times}96$ and lattice spacing determined at a $\simeq 0.093$ fm [9]. The parameters of the calculation are summarized in Table 1. This setup allows calculation of G_E on all five sink-source separations and of G_M, G_A and G_p on the three smallest. G_E and G_M can be extracted directly via Eq. (2.2) since they depend on different sink projectors. G_A and G_p

t_s [a]	Proj.	$N_{\rm cnf} \cdot N_{\rm src} =$	$N_{\rm st}$
10,12,14	Γ_0, Γ_k	$578 \times 16 =$	9248
16	Γ_0	$530 \times 88 =$	46640
18	Γ_0	$725 \times 88 =$	63800

Table 1: Form factor calculation setup. The first column shows the sink-source separations used, the second column the sink projectors and the last column the total statistics ($N_{\rm st}$) obtained using $N_{\rm cnf}$ configurations times $N_{\rm src}$ source-positions per configuration.

are both extracted from the last expression of Eq. (2.2). We separate the two form factors via an over-constrained fit, solving the resulting eigenvalue problem via singular value decomposition, as explained in Ref. [10].

3. Results

3.1 Axial form factors

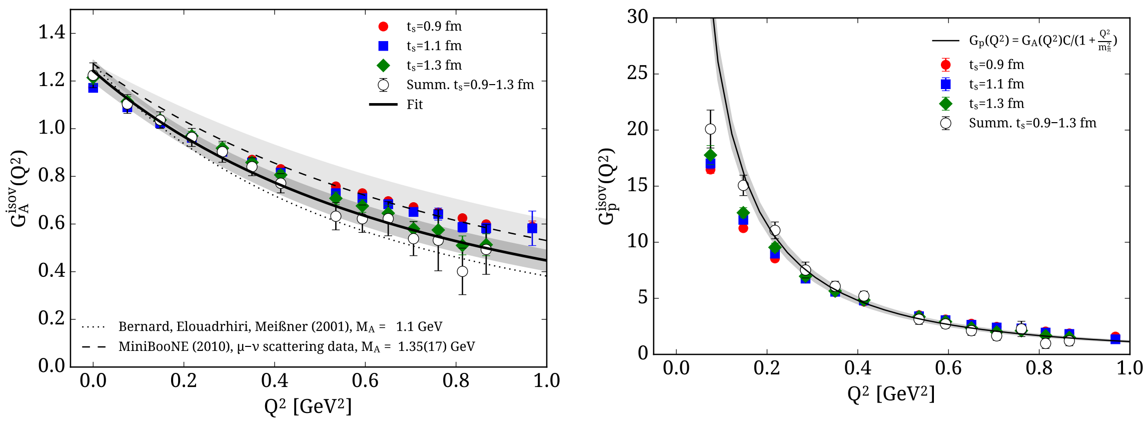

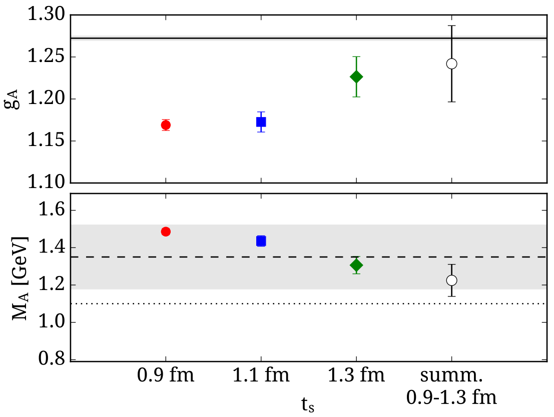

Figure 2: Left: Axial nucleon form factor using $t_s \simeq 0.9$ fm (red circles), 1.1 fm (blue squares), and 1.3 fm (green diamonds) and using the summation method (open circles). The solid line (upper panel) is a fit of the latter to a dipole form. The dashed and dotted lines are from Refs. [4] and [11] respectively. Dipole fit results (lower panel) are compared with g_A from Ref. [12] shown with the solid line. Top: Results for the induced pseudo-scalar form factor G_p with the notation of the left panel.

The axial form factors are shown in Fig. 2. For G_A we see values increasing at low Q^2 as the sink-source separation increases, while at larger momenta we see a decreasing trend. We fit all three sink-source separations, and the summation method, to a dipole form: $G_A(Q^2) = \frac{g_A}{(1+Q^2/M_A^2)^2}$, allowing both the axial charge g_A and the axial mass M_A to vary. We observe g_A approaching its experimental value with increasing sink-source separation. More details on this calculation of g_A

can be found in Ref. [13] in these proceedings. M_A is found consistent within errors of a recent experimental determination [4] shown with the dashed line in the central panel of Fig. 2. We note that our values of M_A are also consistent within the wide error of a recent reanalysis of experimental data, not shown in Fig. 2, which yields M_A=1.01(24) GeV [5].

The induced pseudo-scalar form factor G_p exhibits similar excited-state dependence at low Q^2. Assuming a pion-pole motivates the form: $G_p(Q^2) = G_A(Q^2)C/(1+\frac{Q^2}{m_\pi^2})$ to which we fit to using a dipole form for G_A thus requiring only C to vary. We obtain $\sqrt{C}/2 = 5.9(2)$ to be compared to the phenomenological expectation $\sqrt{C}/2 = m_N/m_\pi = 7.16(4)$ [10].

3.2 Electromagnetic form factors

The isovector electromagnetic Sachs form factors are shown in Fig. 3, where for G_E two additional t_s values are available. For G_E we see a tendency towards the experimental results as t_s increases. The same is not observed for G_M which underestimates the low-Q^2 experimental values and which decreases with increasing t_s.

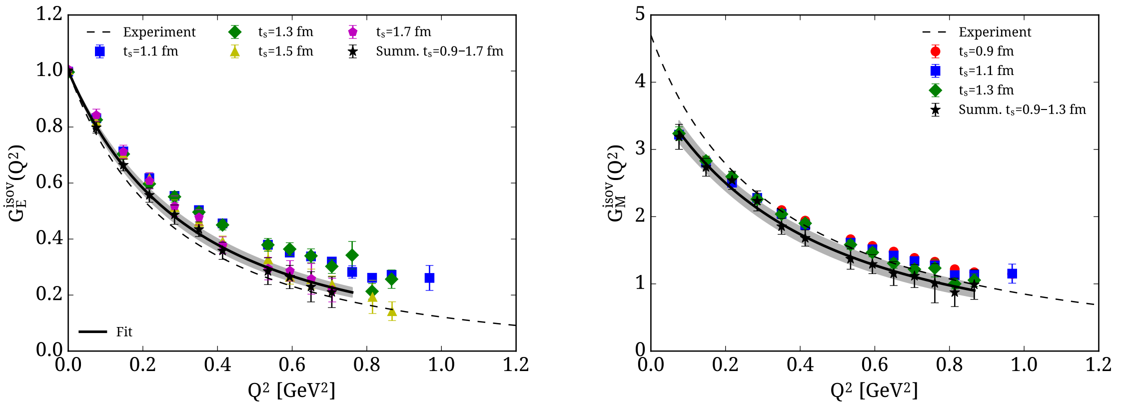

Figure 3: Isovector electric (left) and magnetic (right) Sachs form factors. For G_E we show with yellow triangles and magenta pentagons $t_s \simeq$ 1.5 and 1.7 fm respectively. Asterisks denote the summation method. The solid line and band denotes fits to a dipole form as explained in the text. The dashed line is the experimental parameterization.

The electric and magnetic radii are related to the slope of the form factors at $Q^2 = 0$, namely: $\langle r_i^2 \rangle = -\frac{6}{G_i(0)}\partial G_i(Q^2)/\partial Q^2$, $i = E,M$. We fit all sink-source separations and the summation method to a dipole form $G_i(Q^2) = G_i(0)/(1+\frac{Q^2}{M_i^2})^2$ with $\langle r_i^2 \rangle = \frac{12}{M_i^2}$. For G_E we fix $G_E(0) = 1$ while for G_M we allow $G_M(0)$ to vary. The results are shown in Fig. 4 where for both electric and magnetic radii we see an increasing trend towards the experimentally determined values as t_s increases, while $G_M(0)$ shows mild dependence on t_s.

Our results for the isovector electric and magnetic charge radii are compared to those of other recent lattice calculations in Fig. 5. We see that for both radii lattice results agree within errors and are within at most 2-σ to the experimental values. With further improvement on systematic uncertainties and with increased statistics, contacting experiment is within reach for these quantities.

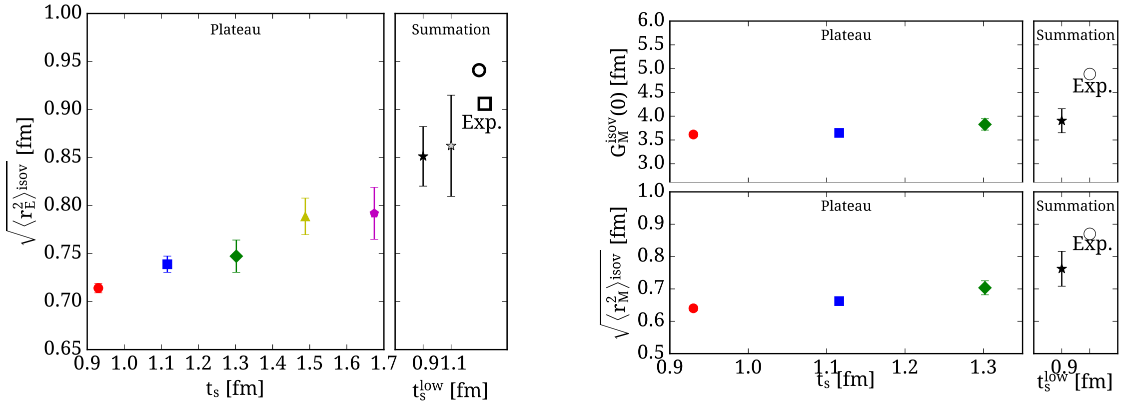

Figure 4: Results for isovector $\langle r_E^2 \rangle$ (left) and $\langle r_M^2 \rangle$ (bottom right) and $G_M(0)$ (top right) from dipole fits. Fits to results using the plateau method are shown with the symbol notation of Fig. 3. For the summation method we fit all available t_s to obtain the filled asterisk and starting from 1.1 fm using the open asterisk. The open circles are the experimental result from Ref. [1] while the open square from Ref. [2].

4. Summary and conclusions

The isovector axial and electromagnetic form factors of the nucleon have been calculated on a lattice with physical pion mass at multiple sink-source separations up to $\sim$1.7 fm and for $\mathcal{O}(10^5)$ statistics. We find that excited states increase the axial mass and at separations beyond 1.3 fm our result agrees with experimental measurements.

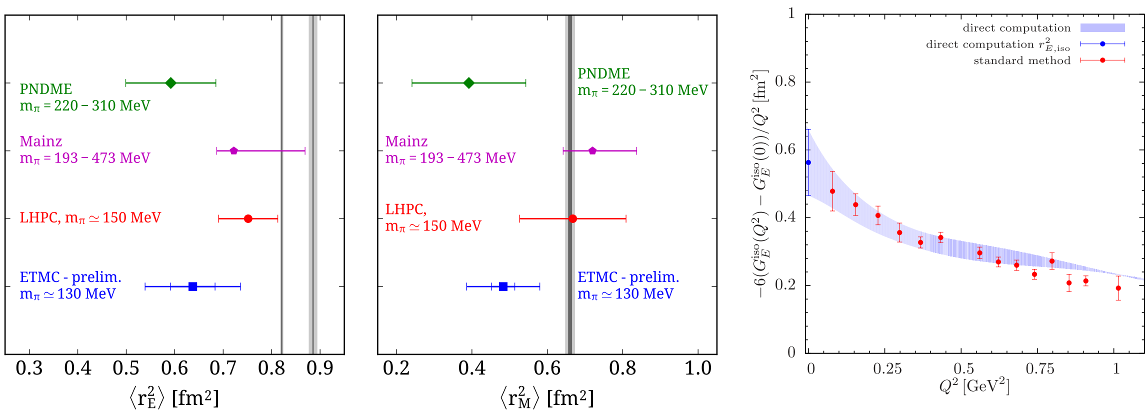

Figure 5: Our results for the isovector $\langle r_E^2 \rangle$ (left) and $\langle r_M^2 \rangle$ (center), shown with blue squares using the plateau method for the largest t_s in each case. The smaller error-bar indicates the statistical error while the larger error includes the systematic uncertainty when considering the summation method. We compare to recent lattice calculations: PNDME [14] (green diamonds), Mainz [15] (magenta pentagons) and LHPC [16] (red circles). The vertical lines show the experimental values also shown in Fig. 4. In the right panel we show a preliminary result of using the position space method of Ref. [17] for determining the slope of $G_E(Q^2)$ for the separation $t_s \simeq$1.7 fm.

The electric and magnetic charge radii show similar behavior, approaching the experimental values with increasing t_s. For $G_M(0)$, the value at $Q^2 = 0$ is underestimated with mild excited state dependence. Calculations at a larger volume, with access to finer momenta, are being carried out to asses the effect on $G_M(0)$.

Recent methods for fitting form factors with no model assumption of the their Q^2 dependence allow for further assessment of systematic uncertainties. In the right panel of Fig. 5 we show the result of applying the position space method of Ref. [17], originally applied for $G_M(0)$, to obtain $\langle r_E^2 \rangle$ at $t_s = 1.7$ fm. At all separations we obtain results for $\langle r_E^2 \rangle$ consistent with what is obtained by the dipole fits shown in Fig. 4. Such methods can benefit from finer momenta using larger lattice volumes, as well as from reduced errors at larger Q^2 using appropriate momentum-dependent smearing as in Ref. [18], both avenues which are currently being explored.

Acknowledgments: Results were obtained using Jureca, via NIC allocation ECY00, HazelHen at HLRS and SuperMUC at LRZ via Gauss allocations with ids 44066 and 10862 and Piz Daint at CSCS via projects with ids s540 and s625. We thank the staff of these centers for access to the computational resources and for their support.

References

[1] P. J. Mohr, D. B. Newell, and B. N. Taylor, Rev. Mod. Phys. **88**, 035009 (2016), 1507.07956.

[2] R. Pohl *et al.*, Nature **466**, 213 (2010).

[3] R. Pohl *et al.*, Science **353**, 669 (2016).

[4] MiniBooNE, A. A. Aguilar-Arevalo *et al.*, Phys. Rev. **D81**, 092005 (2010), 1002.2680.

[5] A. S. Meyer, M. Betancourt, R. Gran, and R. J. Hill, Phys. Rev. **D93**, 113015 (2016), 1603.03048.

[6] ETM, A. Abdel-Rehim *et al.*, (2015), 1507.05068.

[7] A. Abdel-Rehim *et al.*, Phys. Rev. D (in press) (2015), 1507.04936.

[8] ETM, C. Alexandrou *et al.*, Phys. Rev. **D83**, 045010 (2011), 1012.0857.

[9] ETM, A. Abdel-Rehim *et al.*, Phys. Rev. Lett. **116**, 252001 (2016), 1601.01624.

[10] C. Alexandrou, G. Koutsou, T. Leontiou, J. W. Negele, and A. Tsapalis, Phys. Rev. **D76**, 094511 (2007), 0706.3011, [Erratum: Phys. Rev.D80,099901(2009)].

[11] V. Bernard, L. Elouadrhiri, and U.-G. Meissner, J. Phys. **G28**, R1 (2002), hep-ph/0107088.

[12] C. Patrignani, Chin. Phys. **C40**, 100001 (2016).

[13] C. Alexandrou *et al.*, PoS **LATTICE2016**, 153 (2016).

[14] T. Bhattacharya *et al.*, Phys. Rev. **D89**, 094502 (2014), 1306.5435.

[15] S. Capitani *et al.*, Phys. Rev. **D92**, 054511 (2015), 1504.04628.

[16] J. Green *et al.*, Phys.Rev. **D90**, 074507 (2014), 1404.4029.

[17] ETM, C. Alexandrou, M. Constantinou, G. Koutsou, K. Ottnad, and M. Petschlies, (2016), 1605.07327.

[18] G. S. Bali, B. Lang, B. U. Musch, and A. Schäfer, Phys. Rev. **D93**, 094515 (2016), 1602.05525.